Oceanographic–topographic interactions in acoustic propagation in the Iceland–Faeroes front region

Jessie C. Carman[a] and Allan R. Robinson
Division of Applied Sciences, Harvard University, Cambridge, Massachusetts 02138

(Received 26 April 1992; revised 27 October 1993; accepted 4 November 1993)

Effects of oceanographic variation with distance on long-range, low-frequency acoustic propagation in the Iceland–Faeroes front region of the ocean are considered in the presence of realistic topographic variations. A numerical model using a parabolic approximation to the Helmholtz equation, a fluid sediment parametrization and variable topography, is used to calculate acoustic propagation. Oceanographic sound-speed fields output from the Harvard Open Ocean Model, supplemented by climatology in deep regions, provide input sound-speed profiles. Two different propagation transects are considered, both running from shallow to deep water across a developing eddy and across the front. Source depths near the surface, middle, and bottom of the shallow starting profile are studied. Some cases of near invariance to oceanographic changes are found, as are other cases of locally large oceanographic effects (> 30 dB).

PACS numbers: 43.30.Bp, 43.30.Pc

INTRODUCTION

Oceanographic fronts and eddies are mesoscale features that separate or enclose water masses of different properties (e.g., temperature and salinity). They form the oceanic analog of weather systems within the atmosphere; they contain more energy than any other form of motion in the sea and have dominant spatial scales of tens to hundreds of kilometers and dominant temporal scales of days to weeks to months (Robinson, 1983).

Fronts and eddies have been studied extensively within the oceanographic community, and their effects on long-range sound propagation have begun to be explored (Potter and Warn-Varnas, 1991). Lawrence (1983) studied the acoustic effects of warm-core eddies in the Tasman Sea, noting surface ducted sound in the eddy converting to convergence zone propagation outside the eddy, and a change of convergence zone location. Lee *et al.* (1989) demonstrated convergence zone shifts of 5–10 km in acoustic propagation across Gulf Stream eddies, and Mellberg *et al.* (1990) showed that the changing ocean structure within a few days can cause convergence zone shifts of up to 10-km range and magnitude changes of up to 5 dB in a Gulf Stream meander. Sediment and topographic effects were ignored in these studies.

Previous work in acoustic sediment interactions (Frisk *et al.*, 1986; Kuperman and Jensen, 1980) has stressed inference of geoacoustic parameters from near-bottom acoustic propagation patterns and bottom loss information; such work concentrated primarily on the sediment and used simplified (isovelocity) sound-speed profiles in the water. Other work (Hamilton, 1980) has discussed determination of sediment acoustic properties from physical characteristics such as grain size and composition. Relatively little work has been done to study the long-range, large-scale effects the sediment has on propagation patterns. For such long-range calculations, the oceanographic and topographic variations can be expected to play a major role.

Work on the acoustic effects of oceanographic features including interactions with topographic variations, in the presence of a realistic sediment model, is still in preliminary stages. Siegmann *et al.* (1990) showed that inclusion of a fluid sediment layer had a larger effect on propagation patterns in the Gulf Stream region than did inclusions of three-dimensional effects, except in regions of strong azimuthal topographic variations. This led Carman (1991, 1994) to carry out an extensive sensitivity study for the dependence of water column propagation to sediment propagation parameters. Jensen *et al.* (1991) modeled acoustic propagation across the Iceland–Faeroes front, which is topographically tied to the continental ridge and thus occurs in a region of rapidly varying topography. Although the ridge top is relatively flat, there are steep slopes on either side. That work found that inclusion of correct topographic variations had the largest effect on acoustic propagation patterns in the Iceland–Faeroes front region; oceanographic variations produced significant but lesser changes to the sound field. These strong environmental effects on low- to mid-frequency sound propagation were demonstrated using propagation loss curves at specific depths generated by a parabolic approximation model. Ray calculations (essentially a high-frequency approximation) through the same environment provided some physical interpretations for the difference observed, but only for some effects.

The present study draws conclusions again based on propagation loss curves generated by a parabolic approximation model; contour plots of the same model outputs provide low-frequency physical interpretations for the differences seen. Additionally, this work uses a more accurate

[a]Present address: Submarine Development Squadron Twelve, Naval Submarine Base, New London, Groton, CT 06349-5200.

 0001-4966/94/95(4)/1882/13/$6.00

sediment model than in previous long-range interaction studies.

Advances in oceanographic knowledge and field estimation methodology, together with enhanced computing resources, make increasingly realistic simulations of oceanic acoustic propagation possible. Realistic environmental processes can be researched both regionally, and by synthesis, generally by simulations with parametric variations and sensitivity studies. Such simulation studies complement experimental and theoretical studies. This study focuses on frontal, topographic, and sediment effects and interactions in the Iceland–Faeroes region. Low-frequency propagation is studied which minimizes some neglected effects such as arise from small scale sound-speed inhomogeneities and sea surface roughness. Consistently, the parabolic equation approximation is utilized.

For useful range-dependent acoustic calculations, range-dependent sound-speed profiles must be provided. The Harvard nowcast/forecast dynamical model hierarchy (Robinson, 1992) is a set of models that assimilate real ocean data via initialization and updating. They provide realistic four-dimensional field estimates including real-time nowcasts and forecasts as well as hindcasts and data driven simulations. The eddy-resolving water column model dynamics may be either quasigeostrophic or primitive equation, and both types have been applied to dynamical and forecasting studies of the Iceland–Faeroes front (Robinson *et al.*, 1989). The quasigeostrophic (QG) Harvard Open Ocean Model (HOOM) (Miller *et al.*, 1983; Robinson and Walstad, 1987) has been tuned for meandering and eddying of the frontal system over the top of the ridge (Denbo and Robinson, 1988a,b) and the QG-HOOM field estimates together with climatology in the deeper regions provide the basis of the sound-speed estimates for this study. The HOOM outputs provide such sound-speed data sets by using the quasigeostrophic streamfunction to calculate vertical displacements from background density surfaces throughout the domain; the displacements are then applied to background temperature and salinity profiles (Robinson *et al.*, 1994). Sound speeds are calculated using standard formulas (Fofonoff and Millard, 1983).

Acoustic propagation can be calculated in these sound-speed fields, using the Implicit Finite Difference (IFD) model developed at NUSC, New London (Lee and Botseas, 1982; Botseas *et al.*, 1983, 1989). The model uses the parabolic approximation to the Helmholtz equation in two dimensions; it updates the sound-speed profile used with every range step and vertically interpolates between vertical oceanographic model levels using a spline fitting routine (Akima, 1970). Propagation transects have been chosen nearly perpendicular to oceanographic gradients in order to minimize three-dimensional effects. The present version of the model is capable of handling a fluid sediment model with variable topography, although the water–sediment interface is modeled as locally flat (Siegmann *et al.*, 1990). At the interface a sound-speed discontinuity is applied and maintained constant throughout the calculation. Below the interface, the sediment density is set at a new (constant) value, and the sound speed increases linearly with depth to the bottom of the sediment layer. Attenuation is modeled via an imaginary component of the sound speed.

I. OCEANIC REGION, ACOUSTIC TRANSECTS AND SIMULATION PARAMETERS

The geographic region of this study includes the Iceland–Faeroes ridge top and a southern part of the Norwegian Sea. A relatively flat extension of the continental shelf at a depth of about 400 m runs between Iceland and Great Britain, which drops off sharply to the ocean basin on either side. The Iceland–Faeroes front is a permanent water mass boundary that is trapped to the topographic shelf and tilts vertically toward the Norwegian Sea; perturbations to the flow cause meanders and eddies to form. The flow is generally from west to east, with magnitudes which peak between 25–50 cm/s. The conjunction of the two physical features, the hydrographic front and the steep topographic slope, profoundly affects acoustic propagation in the region.

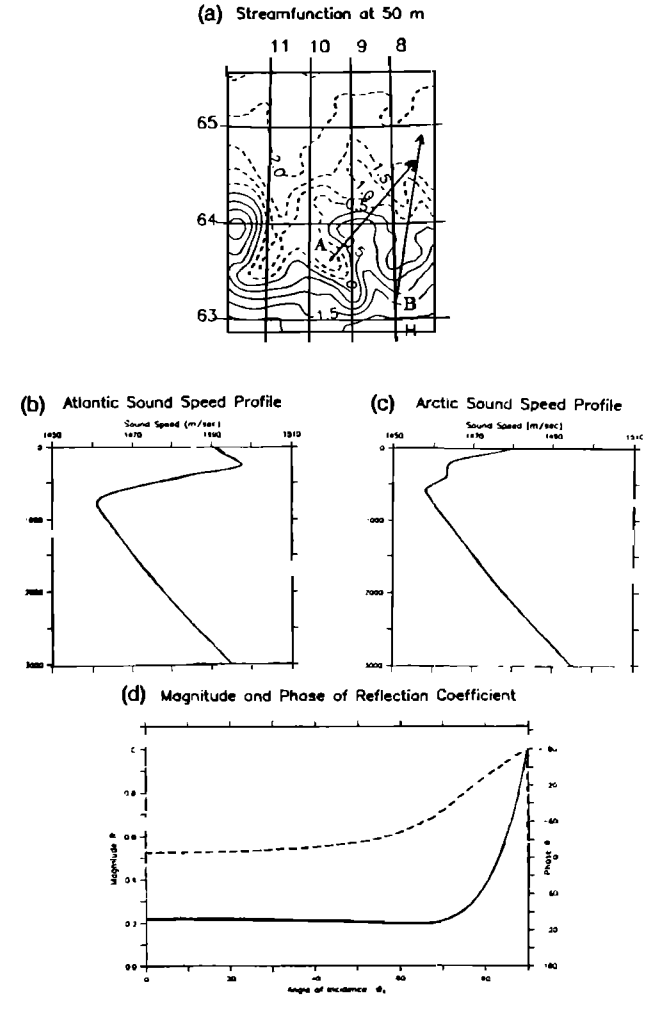

FIG. 1. (a) Gap region quasigeostrophic streamfunction fields at 50-m depth, day 10. Transect A: propagation across a developing eddy. Transect B: propagation across the front. (b) Atlantic water sound-speed profile. (c) Arctic water sound-speed profile. (d) Magnitude and phase of Rayleigh reflection coefficient, $\rho=1.6$, $c_w/c_b=1.031$, $\beta=4.8$.

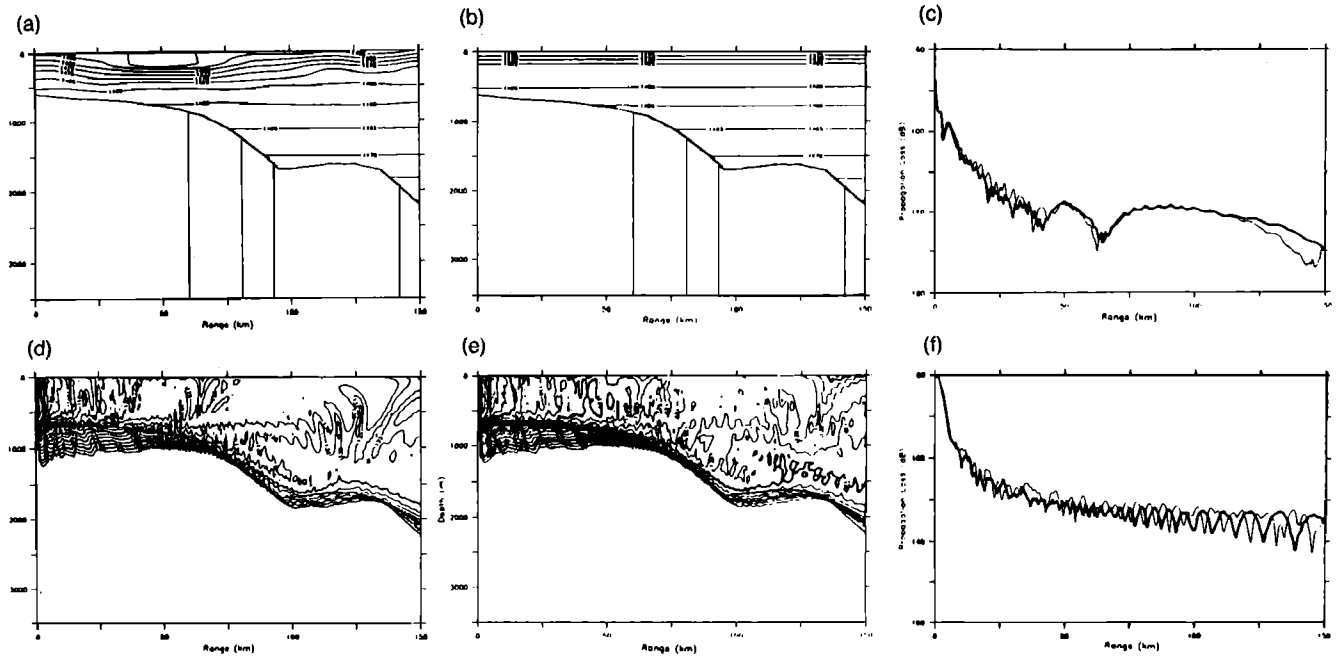

FIG. 2. Comparison of propagation through eddy, with propagation through Arctic sound-speed profile; realistic topography. $z_s = 10$ m, $f = 50$ Hz. (a) Range-dependent sound-speed contours. (b) Arctic profile sound-speed contours. (c) Propagation loss at 10-m receivers, eddy case bold. (d) Range-dependent contours of propagation loss. (a) Range-independent contours of propagation loss. (f) Propagation loss at 600-m receivers, eddy case bold.

In the Iceland–Faeroes front region, data used to initialize the HOOM generally consists of AXBTs (airborne expendable bathythermographs) which provide profiles of temperature with depth (Robinson *et al.*, 1989). These profiles are then supplemented by a climatological temperature-salinity correlation; GEOSAT altimetric data provides additional information on both location and strength of the front. (Robinson *et al.*, 1989; Robinson and Dobson, 1989). The sparse mapping of AXBT data generally limits the resolution of the front in the initialization; the Harvard model has been shown to strengthen dynamically local gradients and improve the frontal resolution (Denbo *et al.*, 1988). Acoustic calculations were performed in day 10 of a model run, to demonstrate phenomena in the more realistic frontal fields. The HOOM was run with an analytic representation to smooth the topography and model levels extending to 850-m depth. Since the sound-speed profiles are primarily downward refracting to this depth, information on the deep profile was required to properly characterize the sound-speed increase with pressure in the deep regions. All of the deeper locations within the model domain fall on the northeastern side of the ridge and thus within the Arctic water mass; therefore, Levitus climatology for that region provided the necessary deep temperature and salinity values for calculations of sound speed (Levitus, 1982).

Acoustic propagation was calculated in the Iceland–Faeroes Gap region under several conditions, ten days after the model was initialized with AXBT data obtained on 26 August 1987. Calculations were performed along two transects, both of which start in shallow water on the ridge and march into the deeper water of the Norwegian basin, over the steep topography. One transect contained a developing eddy midway along its extent, and the other crossed the main Iceland–Faeroes front. Figure 1(a) shows contours of quasigeostrophic streamfunction at 50-m depth (a nondimensional field proportional to dynamic height), with the two propagation transects indicated. [The bottom topography along each transect can be seen on Figs. 2(a) and 5(a), respectively.] In addition, propagation results were calculated using these range-dependent oceanographic fields and flat topography, both shallow and deep, with the results confirming those of Jensen *et al.* (1991) that the topography plays a dominant role in determining the acoustic propagation patterns, with lesser but significant modifications by the oceanography. Due to the extensive length of propagation over shallow topography along these transects, we can expect propagation patterns to be substantially different from those typically seen in deep ocean regimes, where the increase in sound speed with pressure (depth) causes the sound to refract back toward the surface. Calculations were performed at frequencies of 25 and 50 Hz, with source depths of 10, 300, and 600 m (near the top, middle, and bottom of the shallow starting profiles).

In an effort to separate what aspects of the propagation were due to oceanography and what due to topography, the range-dependent oceanographic calculations were compared with range-independent oceanographic calculations. A pair of sound-speed profiles was selected that were typical of the Atlantic water and the Arctic water in this region, and which closely resembled either starting or perturbing profiles for these transects, allowing for profile truncation in shallow topography.

The two typical sound-speed profiles are shown in Fig. 1(b) and (c). The Atlantic sound-speed profile, Fig. 1(b),

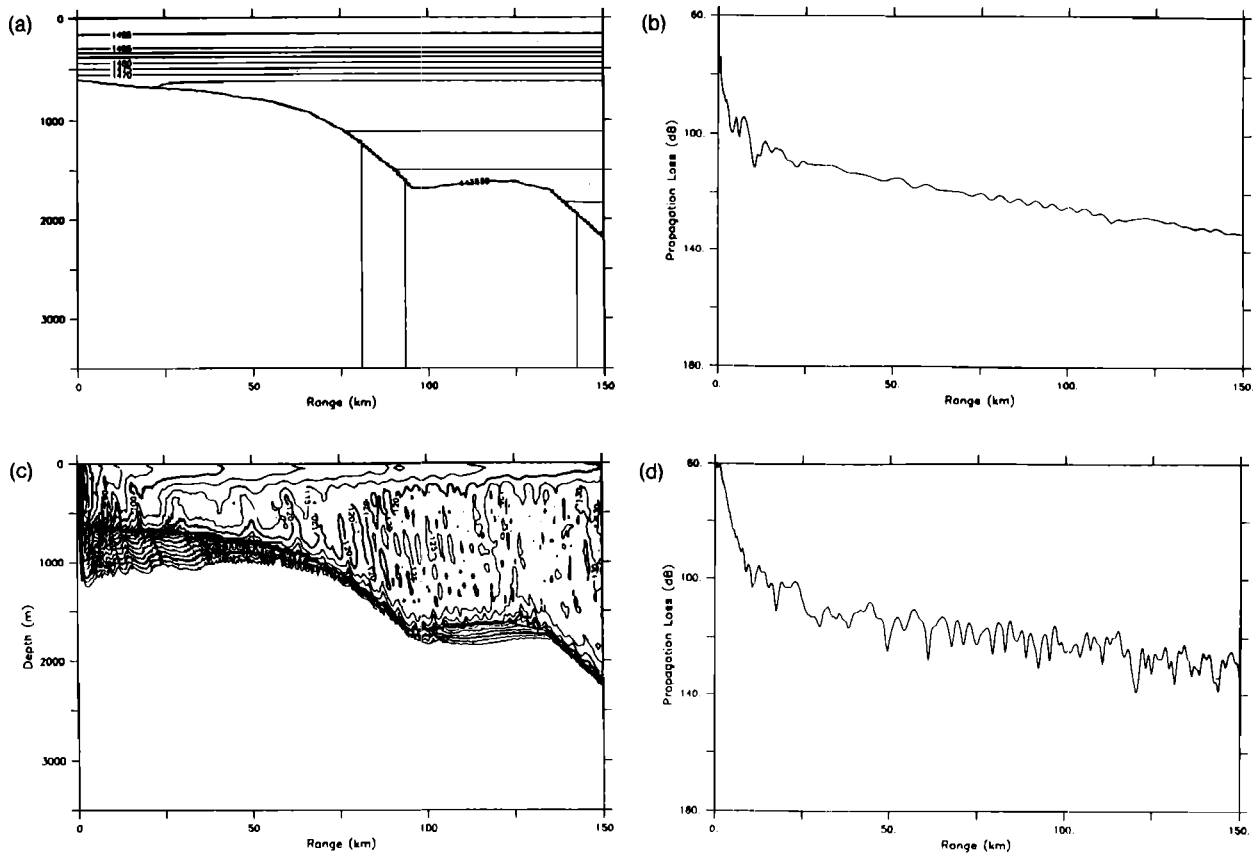

FIG. 3. Propagation through Atlantic profile, realistic topography. $z_s = 10$ m, $f = 50$ Hz. (a) Sound-speed contours. (b) Propagation loss at 10-m receiver. (c) Contours of propagation loss. (d) Propagation loss at 600-m receiver.

shows a deep surface duct to 250-m depth; according to Porter *et al.* (1990) this is consistent with mixed layer depths observed by weather ships in the region. Using the formula $f = 1500/(0.008h^{3/2})$ to estimate the lowest frequency for which the duct will trap sound (Porter *et al.*, 1990; Urick, 1983) we calculate 47 Hz as the lower bound for duct trapping, although the transition between trapping and non-trapping behavior will be somewhat nebulous. The Atlantic sound-speed profile has a deep sound channel near 780-m depth; additionally we note that for most depths in this region (2500 m or less) the relatively high sound speeds in the surface layers ensure that propagation with this profile will be strongly bottom interacting. The Arctic sound-speed profile shown in Fig. 1(c) has a much shallower sound channel axis, near 590-m depth, with another much weaker duct near 305-m depth. This secondary duct has a magnitude of 0.07 m/s and does not trap sound, although it does affect refraction patterns.

Hamilton (1980) has shown that among the most important sediment acoustic properties are density, water–sediment interface sound-speed ratio, sediment sound-speed gradient, depth, and attenuation, and that these properties are more closely associated with sediment type than with topographic depth or location. The sediment parameters selected for this region were density $\rho = 1.6$ g/cm^3, attenuation $\beta = 4.8$ dB/λ6, interface sound-speed discontinuity $c_w/c_b = 1.031$, sediment sound-speed gradient $\partial c/\partial z = 0.5\ \mathrm{s}^{-1}$, and sediment depth $z_{\mathrm{sed}} = 5$ m. Values were obtained from Frisk *et al.* (1986) from their shallow site, in order to characterize the shallow, more strongly bottom-interacting sediment regions more accurately. Figure 1(d) shows the magnitude and phase of the water-sediment Rayleigh reflection coefficient for this parametrization; note that these conditions are strongly reflecting for sound at all angles of incidence, while sound near grazing incidence will again approach 100% reflection. As these parameters remain constant throughout the calculation, the functional form of the reflection coefficient will remain constant with range.

The value of β used in this work is extremely high and is used to model compressional wave conversions to shear waves at the shallow sediment-substrate layer, and subsequent shear wave attenuation (Vidmar, 1980; Knobles and Vidmar, 1986). We note that in a realistic sediment this shallow, we could expect compressional wave reflections off the sediment–basement interface; these reflections were not included in the IFD model of the sediment since we maintain a constant density and sound speed across the perfectly transmitting interface between fluid sediment layer and artificial absorbing bottom. To more realistically handle the situation, a discontinuity in density or sound speed could be used across the interface, or another layer added.

For propagation across the developing warm eddy, the most meaningful comparison was to propagation in the range-independent Arctic profile; the eddy can be thought

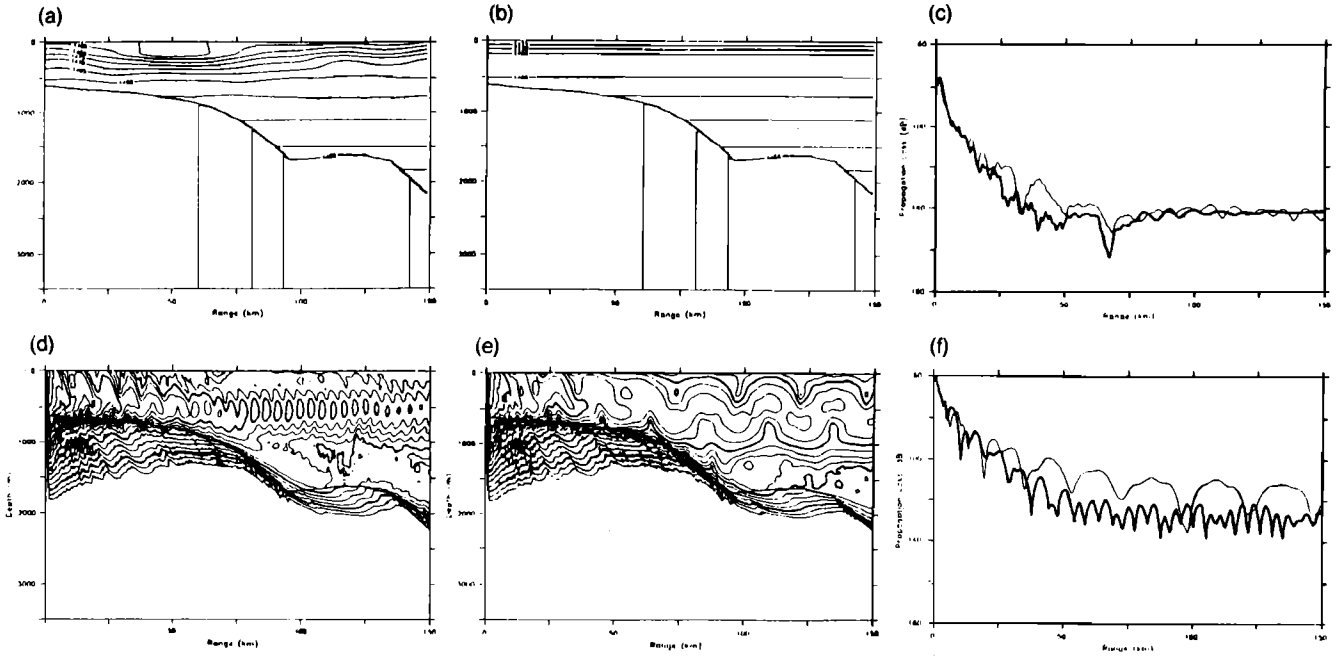

FIG. 4. Comparison of propagation through eddy, with propagation through Arctic sound-speed profile; realistic topography. $z_s=600$ m, $f=25$ Hz. (a) Range-dependent sound-speed contours. (b) Arctic profile sound-speed contours. (c) Propagation loss at 10-m receivers, eddy case bold. (d) Range-dependent contours of propagation loss. (e) Range-independent contours of propagation loss. (f) Propagation loss at 400-m receivers, eddy case bold.

of as a perturbation to the Arctic water mass. For propagation across the frontal transect, comparisons to propagation through both the Arctic and Atlantic profiles proved informative.

Propagation patterns in the Gap region in any case appear to be a balance between whichever is the strongest of several factors. First, the higher the sound speed at the source is relative to that at the sediment, the more important will be the bottom interactions to the entire water column propagation patterns. Conversely, the closer the source is to the sound channel axis, the more strongly excited will be the modes that make up shallow-angle sound paths near the channel axis. Additionally, the Atlantic water surface duct will overwhelm other surface phenomena at $f=50$ Hz but will only serve to increase the surface sound speeds at $f=25$ Hz. Propagation in each case seems to be governed by the relative strengths of each of these effects, for each source location and frequency. An exact determination of the interplay would require closer study with a simplified topography.

Several points can be noted about the topographic effects; first, over the starting shallow regions, the sound will undergo an extremely large number of bottom interactions. In view of the different angles of these interactions, the sound will not be in coherent unidirectional beams when the topography slopes away. Rather, at each location magnitudes will be due to sound travelling along various different paths. Additionally, the angular dependence of the Rayleigh reflection coefficient means that sound in shallower propagation paths will persist to longer ranges than will sound in steeper paths; while over the shallow topography such sound both undergoes fewer bottom interactions and incurs less loss with each interaction. Thus the shallow starting range acts to selectively filter out the steeper propagation paths from the sound field.

II. PROPAGATION THROUGH THE WARM EDDY

A. Shallow source

When the realistic topography is used for calculations with different oceanographic conditions, the result is a complex array of propagation patterns about which generalization is difficult. In many cases, a pattern of magnitudes appeared in the shallow receiver ($z_{\text{rcvr}}=10$ m) that was almost invariant to oceanography but which depended on topography. Figure 2 shows an example of this invariance by comparing propagation through the eddy at $f=50$ Hz, source $z_s=10$ m with propagation from the same source with the same frequency through the Arctic profile. Receiver depths in these figures are 10 and 600 m; the eddy receivers are bold. Note in the 10-m receivers, the pattern of minima near 40- and 65-km range with a broad maximum in between, followed by that broad maximum extending between 75 and 125 km. This occurs geographically coincident with the warm eddy, and might be considered an effect of the oceanography, except that the range-independent Arctic case does not contain the eddy perturbation. Other sources show a similar pattern in the shallow receiver; there may be slight modifications but it is nearly always present, especially the minima near 40- and 65-km range. Because of its relative invariance to oceanography and dependence of topography, it seems to be due to a broad reflection of the incoherent sound off the sloping shelf and the particular reinforcing patterns of the superimposed sound. A different form of topographic pattern occurred in the range-dependent and range-independent

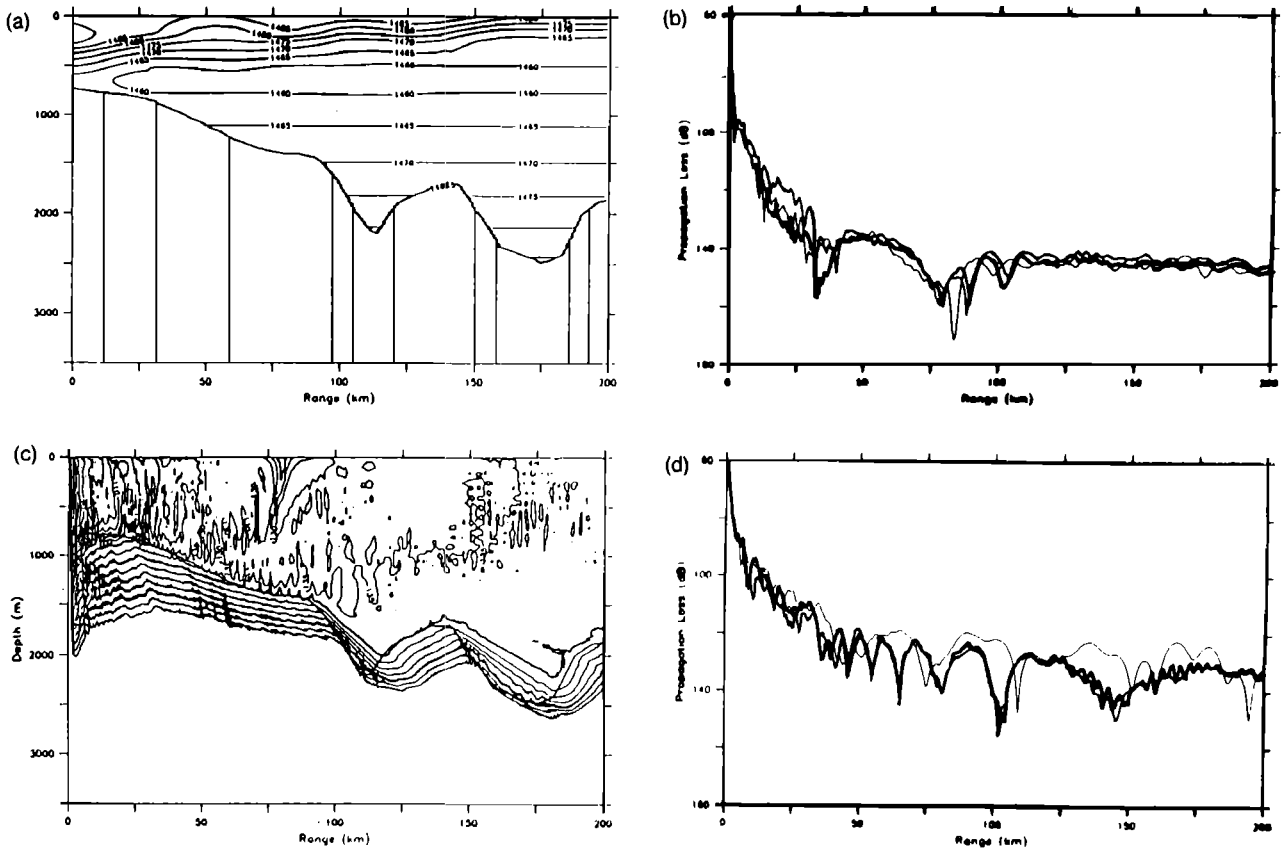

FIG. 5. Propagation across front, realistic topography. $z_s = 10$ m, $f = 25$ Hz. (a) Sound-speed contours. (b) Propagation loss at 10-m receivers, frontal case bold, Atlantic case medium, Arctic case light. (c) Contours of propagation loss. (d) Propagation loss at 250-m receivers, frontal case bold, Atlantic case medium, Arctic case light.

oceanographic calculations along transect B; the topography proved too irregular to attach a specific interpretation to these patterns. These patterns will be pointed out in the upcoming examples. At 25 Hz for this case, a similar pattern of topographic interactions dominated the entire water column propagation.

Propagation along this transect with the Atlantic water profile (Fig. 3) and 10-m source at 50 Hz shows an example of the primary instance in which the oceanographic effects overwhelmed this topographic effect. Recall that for a surface duct of 250-m depth, we can expect surface trapping for sound at 47 Hz and above; in Fig. 3(c) we see sound propagating to long distances in the upper region of the water column. Note in the 10-m receiver the greatly enhanced sound levels over the other two cases, Fig. 2(c) of the 10-m receivers in the eddy and Arctic profiles. This surface trapping is sufficient to overwhelm any topographic effects seen in the shallow receiver, whenever it occurs.

B. Near bottom source

Propagation through the eddy with the source near the bottom of the shallow-water profile ($z_x = 600$ m) at $f = 25$ Hz showed an interesting effect of the interaction of oceanography with topography. Figure 4 compares this case with the corresponding case of propagation through the Arctic profile. Receivers shown are at 10- and 400-m depth. In the 10-m receivers, we see the form of topographic interaction typical of this bottom configuration and frequency; note the minima near 65-km range preceded by a weak maximum near 55 km, followed by broad maxima. At 25 Hz, we do not see a magnitude decrease near 150-km range. In the contours of propagation loss for propagation through the eddy we can see the effects of the downward refraction of the eddy between 35- and 60-km range as the sound refracts away from the surface. As we saw in the shallow, flat-bottom case, this will cause an increase in bottom interactions and thus an increase in loss, even of sound that used to be propagating at shallow angles. Indeed, when the bottom topography deepens near 75 km the propagation pattern found in the sound channel appears to be dominated by a single mode propagating down the center of the channel, with magnitude between 120–125 dB by 150-km range; recall that deeper sources will excite the modes propagating near the center of the sound channel more strongly than will shallow sources. Traces of higher modes remain in the modulations to the channel axis pattern. Note also the refracted sound propagation down the topographic slope; this effect was also documented by Jensen and Kuperman (1980a).

The receiver at 400 m shows the small-scale pattern of maxima associated with this single mode, as well as the modulations by other modes. Comparing to the Arctic profile case, we see no such downward refraction near 35 km;

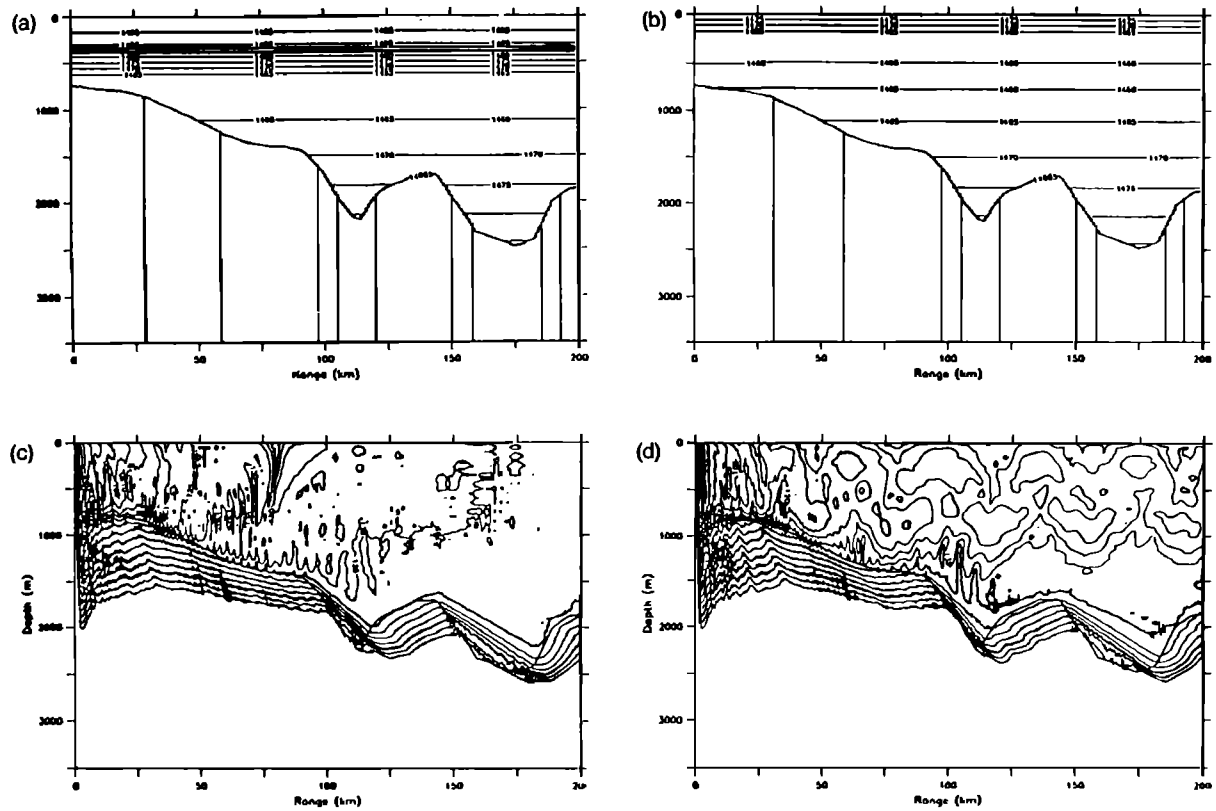

FIG. 6. Propagation through Atlantic and Arctic profiles, realistic topography. $z_s=10$ m, $f=25$ Hz. (a) Sound-speed contours, Atlantic profile. (b) Sound-speed contours, Arctic profile. (c) Contours of propagation loss, Atlantic profile. (d) Contours of propagation loss, Arctic profile.

instead the topography simply removes the more steeply propagating sound leaving the sound in more shallow paths. Thus after the topography deepens near 75-km range, more sound remains in the sound channel at a wider variety of propagation angles, forming broad convergence zones with magnitudes between 100 and 115 dB by 150-km range. The receiver at 400 m shows the broader pattern of maxima associated with the convergence zone pattern, as well as the increased ensonification associated with the lesser loss. At 50 Hz, propagation with the 600-m source past the eddy showed a similar increase in the degree of trapping in the sound channel over the Arctic profile case, although a greater number of shallow angle modes remained near the sound channel at the higher frequency.

III. PROPAGATION ACROSS THE FRONT

A. Shallow source

Propagation through the front along transect B also proved to be a complex interaction of source depth, frequency, and topography about which few generalizations could be made, except to say again that deeper sources more strongly excite shallow-angle sound in the channel axis. With the source at the top of the starting profile, bottom interactions set up at the beginning of propagation dominate the entire range of calculation. Figure 5 shows propagation across the front for a source at 10-m depth at 25 Hz; receivers are at 10- and 250-m depth. The receiver plots contain overlays of the same receivers from propagation across this topography in both the Atlantic sound-speed profile and the Arctic profile; the frontal case is bold, Atlantic case medium, and Arctic case light. From the sound-speed contours we see the typical frontal slant toward the Arctic water; at depth, the frontal contrast is within the first 25 km of calculation, while at the surface it is at approximately 150-km range. Note that propagation along this transect is in primarily Arctic type water; we see no deep surface duct past 15-km range and only the location of strong sound-speed gradient toward the surface changes. In the 10-m receiver we see the form of the topography interaction along this transect with its slightly different bottom configuration; propagation loss with all three oceanographic conditions is nearly identical at this receiver. The minima near 30- and 80-km range, together with the maximum near 50 km, occur in a great number of the cases. Additionally, the receiver at 250-m depth shows great similarity in the propagation patterns between the Atlantic profile and the frontal transect; thus conditions at the beginning of the profile have a very strong effect on propagation. Note the qualitative difference in the Arctic receiver; the destination water mass has relatively little effect on propagation patterns.

Comparing this range-dependent oceanographic case with the propagation contours in either the Atlantic water or the Arctic water (Fig. 6) with the same source depth and frequency again reveals this dependency: propagation through the Atlantic water profile shows the same pattern of bottom interactions and the same qualitative propaga-

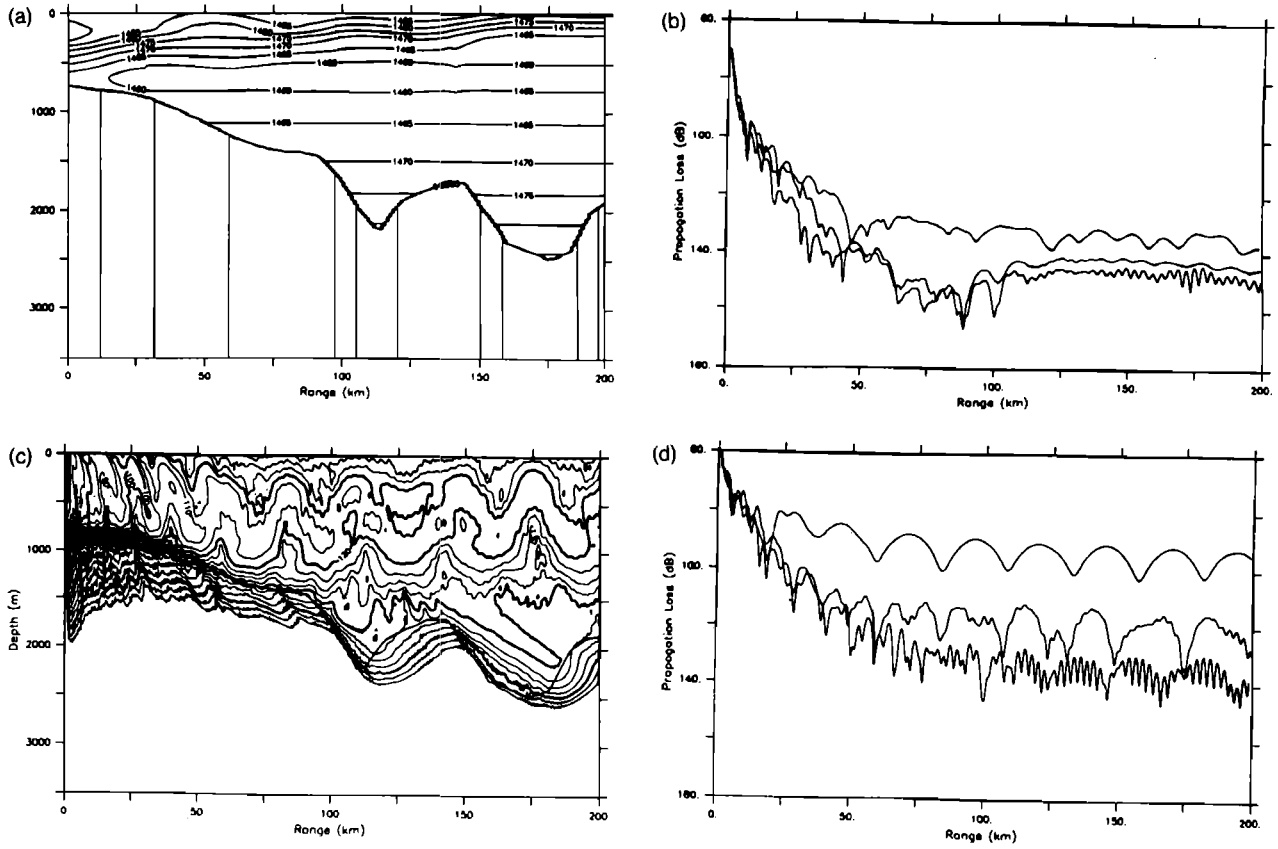

FIG. 7. Propagation across front, realistic topography. $z_s = 300$ m, $f = 25$ Hz. (a) Sound-speed contours. (b) Propagation loss at 10-m receivers, frontal case bold, Atlantic case medium, Arctic case light. (c) Contours of propagation loss. (d) Propagation loss at 750-m receivers, frontal case bold, Atlantic case medium, Arctic case light.

tion patterns throughout the water column as does the propagation across the front. Alternatively, propagation through the Arctic water profile shows a diffuse convergence zone propagation pattern which appears to overwhelm the bottom interactions seen in the other two cases. Note in the Arctic water 250-m receiver that sound levels in the convergence zones are approximately 120–125 dB by 175-km range; sound levels in the 250-m receivers for the frontal oceanography and the Atlantic profile are about 133 dB at the same range. In the Arctic profile, a water-propagating pattern seems to overwhelm the topographic effects seen in both the frontal and Atlantic cases.

We note that for the Atlantic profile, which is most similar to the starting profile of the frontal crossing, the main sound channel axis is near 780-m depth; for the Arctic profile, the main sound channel axis is near 590-m depth and the sound speeds are considerably lower in the upper water column than in the Atlantic profile. The starting bottom depth along this transect is 734 m; thus for the Arctic sound-speed profile there is some very small amount of upward refraction before the bottom is encountered, which the downward topography will increase, permitting water-refracting sound to propagate within close ranges of the source. In the Atlantic sound-speed profile with its deeper sound channel axis, this topography configuration does not permit any water-refracting sound until after 25-km range. In the realistic frontal oceanography, the shallowing of the sound-speed channel in conjunction with the deepening topography permits water-refracting sound after approximately 10 km. Apparently this is not soon enough in the propagation pattern to overwhelm the bottom-interacting sound that makes up those topographic acoustic patterns seen in the shallow receivers, and the resulting propagation patterns into the Norwegian Sea are dominated by the presence of Atlantic water at the source location. At 50 Hz for this source depth, the bottom interactions set up at the beginning of the propagation again dominated the entire calculation. Propagation patterns appeared very sensitive to the conditions in short ranges.

B. Middle source

With the source in the center of the starting water column, a different propagation effect obtains; propagation across the front shows effects of Arctic water, modified by bottom interactions generated near the source. Figure 7 shows propagation across the frontal transect for the source at 300-m depth at 25 Hz with receivers at 10 and 750 m. Overlaid on the receiver plots again are the corresponding receivers from propagation through Atlantic and Arctic sound-speed profile, with frontal case bold, Atlantic case medium, and Arctic case light. In the 10-m receiver we again see the pattern of bottom interactions in both the frontal and Atlantic cases, while the 750-m receivers easily

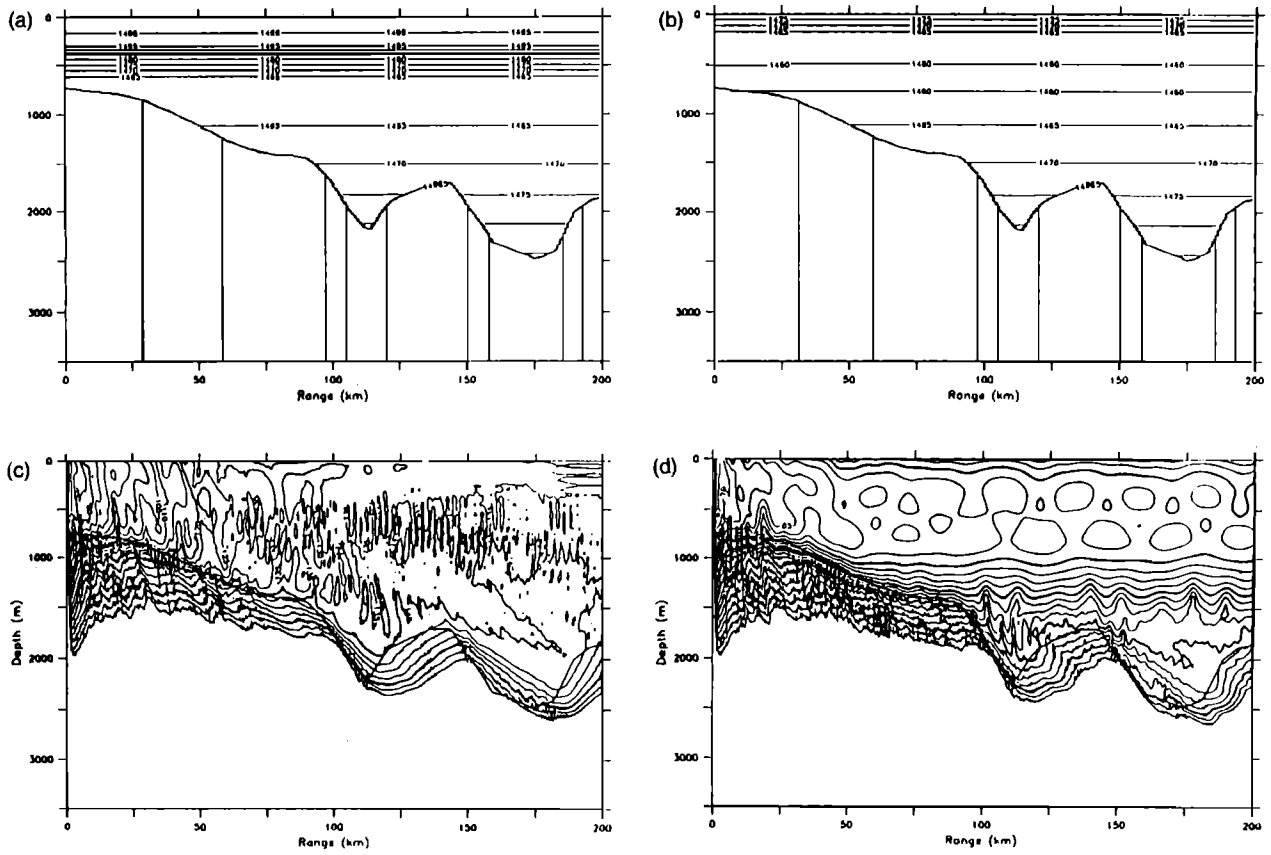

FIG. 8. Propagation through Atlantic and Arctic profiles, realistic topography. $z_s = 300$ m, $f = 25$ Hz. (a) Sound-speed contours, Atlantic profile. (b) Sound-speed contours, Arctic profile. (c) Contours of propagation loss, Atlantic profile. (d) Contours of propagation loss, Arctic profile.

distinguish between the three cases. The contour plot of propagation loss shows a convergence zone propagation pattern within the sound channel, however, as does the receiver at 750-m depth. Comparing this range-dependent case against the matching propagation contours through the Atlantic profile (Fig. 8, left), we see in that case a broad interference pattern that appears to be the bottom interactions that obtain for this topographic configuration and source depth. With matching conditions in the Arctic profile (Fig. 8, right), however, once the topography deepens enough to permit sound channel propagation, significant amounts of sound propagate to long ranges within the channel. The regular pattern formed in the channel axis is reminiscent of the propagation patterns observed by Jensen and Kuperman (1980b) and Collins *et al.* (1988) for their examples of parabolic approximation propagation in shallow water with only the three lowest modes excited; thus the particular choice of source depth in this sound-speed profile with this amount of bottom losses seems to filter out all but a very small number of modes, probably two, in the center of this profile. Traces of other modes exist and can be seen as modifications to the propagation patterns, such as the modulations of magnitude and the small oscillations near 1400-m depth in the contours of propagation loss. It would be interesting to directly calculate the vertical modes for these sound-speed profiles.

We can see a similarity in the locations and forms of these maxima in the Arctic-profile case to the maxima in the convergence zone pattern seen in the realistic oceanographic case, Fig. 7(c). In that case the locations are slightly shifted, and the small-scale oscillations similar to the bottom interacting interference pattern overlay the channel axis propagation. The 750-m receivers clearly differentiate between the Arctic profile pattern of oscillations, the Atlantic profile interference pattern, and the realistic propagation pattern which shows traces of both. Thus for this source depth, the sound in water-propagating paths was strong enough to overwhelm the interference effects caused by the early profile; propagation patterns this time are dominated by characteristics of the destination Arctic water mass, with modifications due to the presence of Atlantic water at the starting location. At 50 Hz with the same source depth, propagation conditions across the front again showed oceanographic effects with an overlay of bottom interaction interference.

C. Near bottom source

When the source is at 600-m depth, it is very close to the Arctic profile 590-m sound channel axis and fairly close to the Atlantic profile 780-m sound channel axis; we can expect strong excitation of shallow-angle sound in that axis. This is indeed the case, as we see in Fig. 9 for the 600-m source at 50 Hz with realistic oceanography; receivers shown are at 10- and 300-m depth. Again, receivers are overlaid with corresponding cases from both Atlantic and

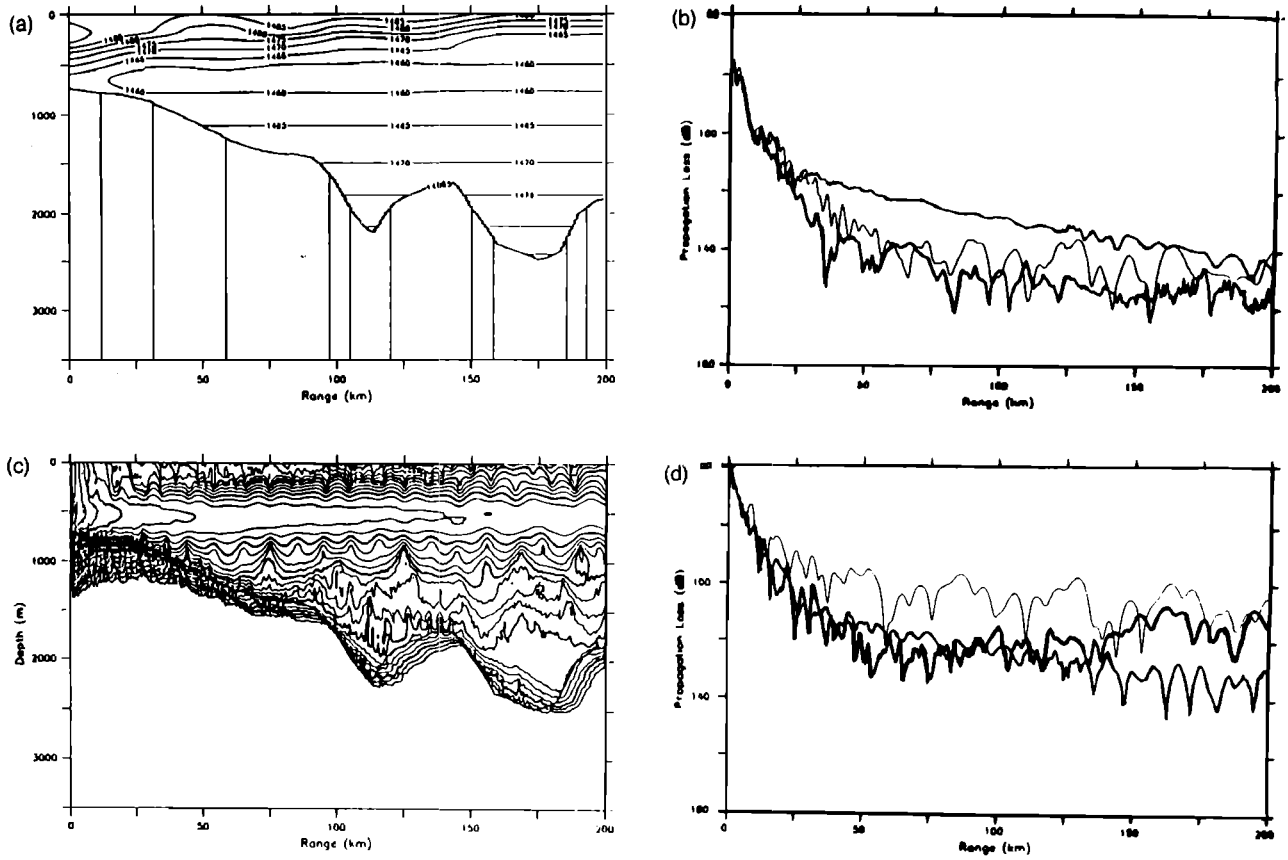

FIG. 9. Propagation across front, realistic topography. $z_s = 600$ m, $f = 50$ Hz. (a) Sound-speed contours. (b) Propagation loss at 10-m receivers, frontal case bold, Atlantic case medium, Arctic case light. (c) Contours of propagation loss. (d) Propagation loss at 300-m receivers, frontal case bold, Atlantic case medium, Arctic case light.

Arctic profiles; the frontal case is bold, Atlantic case medium, and Arctic case light. The contours of propagation loss show the sound to be tightly constrained within the sound channel axis around 600-m depth, with a very small amount of vertical extent. Comparing this case with similar propagation through the Atlantic profile (Fig. 10, left), we see that in the Atlantic profile the strong sound-speed gradient between 300- and 600-m depth, in conjunction with the large amount of loss to steeply propagating sound in shallow regions, has removed propagation paths with large vertical angle and strongly confined the sound to the center of the Atlantic sound channel axis near 750-m depth. Propagation in the range-independent Atlantic sound-speed profile shows sound trapping in the surface duct, which did not appear in the range-dependent case due to the lack of duct beyond 15-km range. Additionally, the Atlantic profile with its steep gradient between 300- and 700-m depth strongly confines sound to the channel axis, while interactions with the early shallow bottom remove steep-angle sound. Range-independent propagation in the Arctic profile (Fig. 10, right), with its shallower sound channel axis and more gradual increase in sound speed toward the surface, permits a greater range of vertical propagation around the center of the sound-speed duct with less bottom loss and thus greater ensonification at a wider range of depths.

As might be believed, the amount of ensonification within the duct in the range-dependent case is intermediate between the duct sound magnitudes seen in either range-independent case; with the range-dependent oceanography, sound levels in the duct range between 90 and 95 dB by 200-km range. With the Atlantic sound-speed profile [Fig. 10(c)] sound levels in the duct are lower, and range between 95 and 100 dB at the same range; the increased bottom losses associated with the stronger surface sound-speed gradient have removed more sound from the propagation pattern. With the Arctic sound-speed profile [Fig. 10(d)] sound levels in the channel axis are higher, and range between 85 and 90 dB by 200-km range, as the weaker sound-speed gradient in the upper profile has decreased the amount of bottom interaction.

The 10-m receivers display these effects; in the frontal case, there is little ensonification of shall regions. The 10-m receiver from the Atlantic profile shows increased magnitudes due to surface ducting, and the Arctic case shows variable increased magnitudes due to the greater range of vertical propagation permitted with that profile. Note in the 300-m receivers that the frontal case shows the same decreased magnitudes due to the strong downward-refracting gradients in the early profile; as the vertical tilt of the Iceland–Faeroes front causes these gradients to shallow, ensonification increases at the 300-m receiver although the greatest sound magnitude remains trapped at the center of the channel. Thus with the source near the

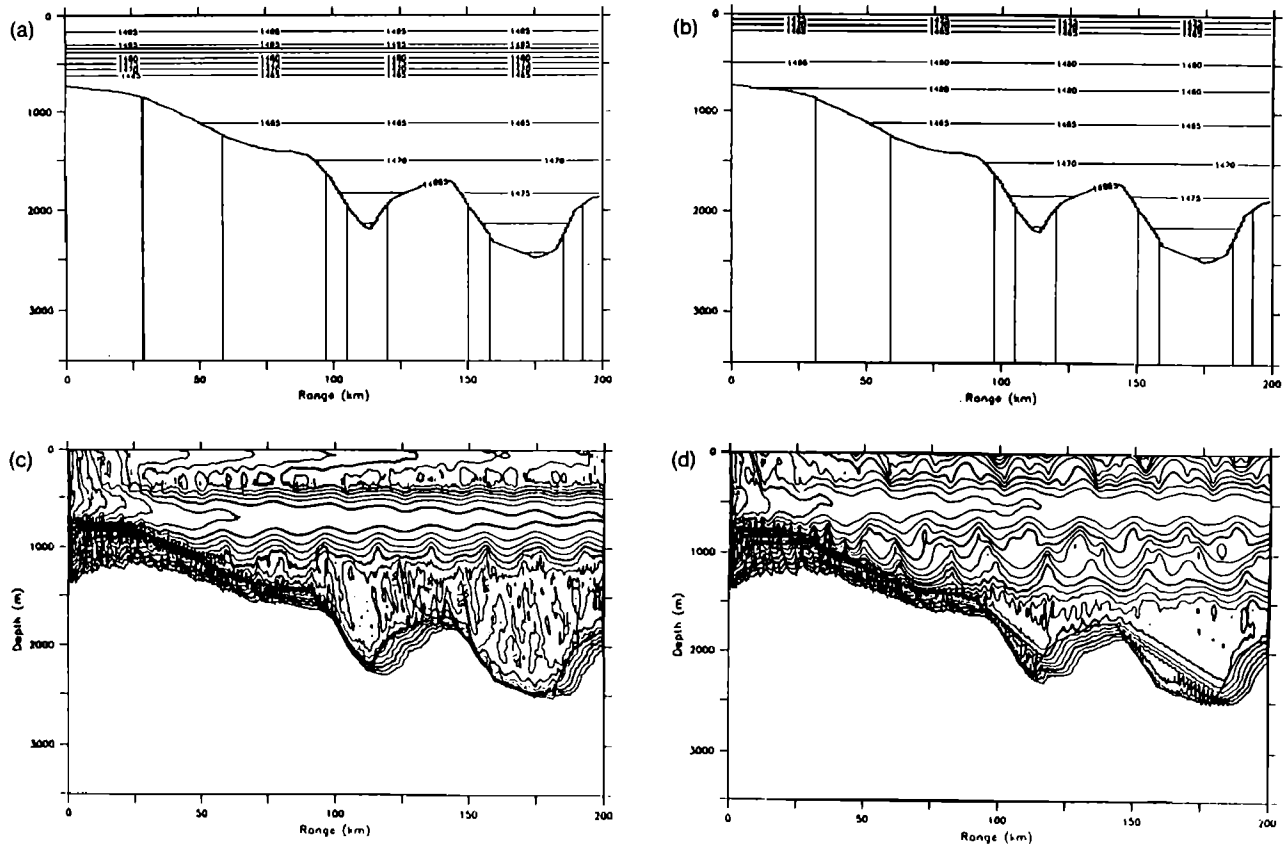

FIG. 10. Propagation through Atlantic and Arctic profiles, realistic topography. $z_s = 600$ m, $f = 50$ Hz. (a) Sound-speed contours, Atlantic profile. (b) Sound-speed contours, Arctic profile. (c) Contours of propagation loss, Atlantic profile. (d) Contours of propagation loss, Arctic profile.

bottom of the starting water column, the strong excitation of shallow angle modes at the center of the channel and rapid extinction of steeper-angle sound due to bottom losses causes propagation to be mostly limited to sound in the channel axis. The location of that channel axis is determined by the destination Arctic water mass; the strong losses are caused by the interaction of the early Atlantic water mass with the shallow topography. Similar results appeared for the 25-Hz case.

IV. SUMMARY

Propagation within the Iceland–UK Gap region has been shown to be extremely varied and is difficult to generalize, but is governed by the interactions of several effects. First, due to the large horizontal range of propagation in a downward-refracting profile over shallow topography, the sound undergoes an extremely large number of bottom interactions with different repeat distances and incident angles; when the topography deepens, the sound field will not consist of coherent unidirectional beams. Rather, at each location the magnitude will consist of sound travelling along various different paths. These bottom interactions will also preferentially filter out sound with steep propagation paths due to the smaller magnitude of the reflection coefficient for steep angle sound. Changes in the oceanographic sound-speed profile over this shallow topography alter the horizontal frequency of the bottom interactions, and thus adjust the amounts of loss.

Additionally, in many of the calculations shown, a complex propagation pattern appeared that was almost invariant to oceanography and thus was attributed to the topography. The appearance of this pattern was stronger for shallower sources, which were more strongly bottom interacting due to their weaker excitation of shallow-angle modes in the center of the sound channel. The form of this topography induced pattern is not understood due to the complexity of the topographic variations.

Deeper sources closer to the sound channel axis (which was close to the shallow bottom) will excite the shallow-angle modes in the center of the sound channel more; thus their propagation patterns were more strongly affected by the oceanography and its variations with range. Topographic losses still occur over the early propagation range, but their magnitude is less due to the larger amount of shallow-angle sound.

Propagation along the transect containing the developing eddy primarily showed the effects of the increased bottom losses due to the strongly downward-refracting gradient at its base. These increased losses more effectively removed the steep-angle sound than did the oceanographic fields without the eddy. Figure 11(a) schematizes these eddy-induced losses, while Fig. 11(b) shows range-independent fields for comparison. The lines are not intended to depict rays, but instead represent important propagation paths. The increased losses due to the eddy effectively remove all but the shallowest-angle sound in the

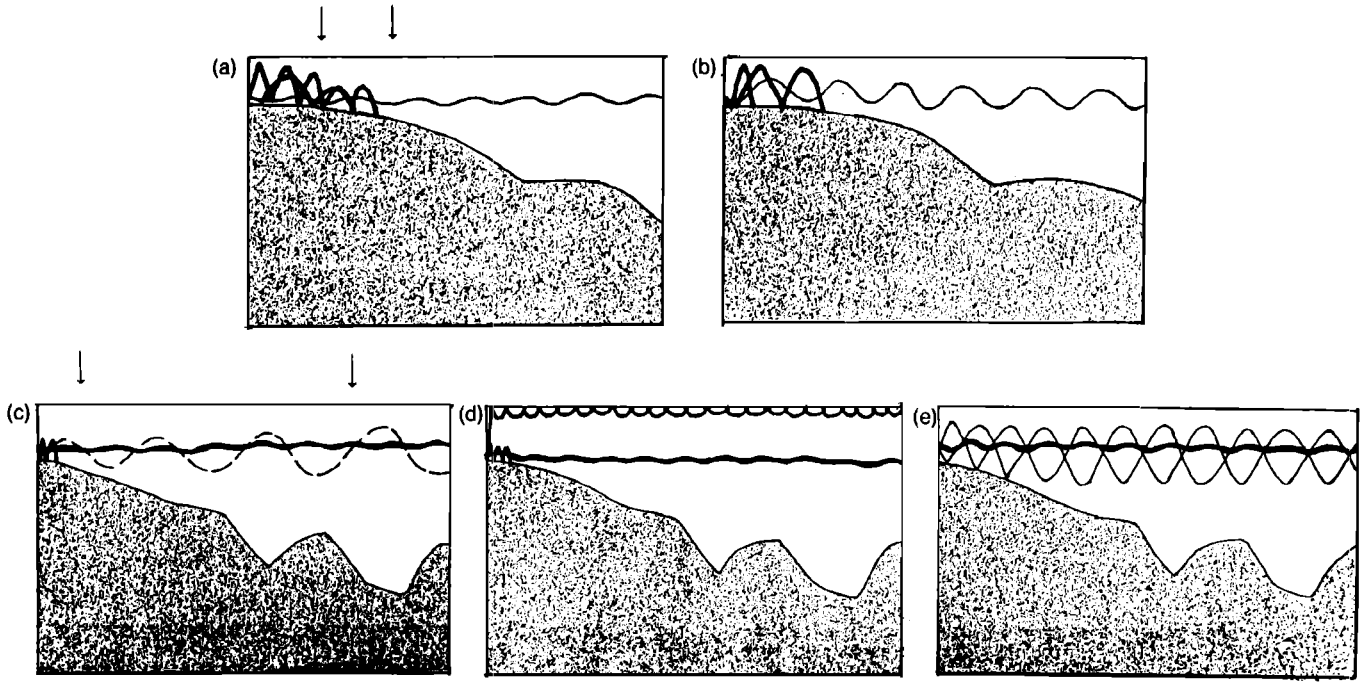

FIG. 11. Schematic of Iceland–UK Gap propagation. (a) Propagation through eddy. Arrows represent start and end of eddy. (b) Propagation through Arctic water sound-speed fields. (c) Propagation across Iceland–Faeroes front. Arrows represent approximate locations of deep and surface front, respectively. (d) Propagation through Atlantic water sound-speed fields. (e) Propagation through Arctic water sound-speed fields.

center of the sound channel, reducing sound magnitudes by 10–15 dB in the channel and 20–25 dB elsewhere. Different source depths will excite different amounts of shallow-angle modes so the propagation pattern will depend strongly on source depth, but the effect of the eddy will always be to remove preferentially the steeper angle sound.

Propagation along the transect across the Iceland–Faeroes front resulted in sound patterns revealing the effects of both water masses, that at the source and that at greater distance. Figure 11(c) schematizes propagation across the frontal transect, showing strong downward refraction due to the deep steep sound-speed gradient in the early Atlantic water mass, followed by propagation closely limited to the center of the sound channel. In Fig. 11(c), the wide-angle long-range path is drawn dashed to indicate that sound did propagate in wider angle paths, but with greatly reduced intensity compared with the shallower angle sound (20–25 dB less).

For comparison, Fig. 11(d) schematizes propagation through Atlantic water sound-speed fields, with the surface duct trapping some sound near the surface and the deep strong gradient which, in conjunction with the shallow topography, strongly confines sound to the channel axis. Figure 11(e) shows propagation patterns in the Arctic water sound-speed fields, with the shallow-angle sound bold and the wide-angle sound light, to indicate relative intensities. Comparing propagation across the front with the two range-independent cases, we see that the early Atlantic-type sound-speed profile strongly confined sound to the channel axis, but that channel axis slowly became shallower on the Arctic side of the front. The transition to Arctic-type water with its shallower surface gradient permitted some wider angle sound to propagate, but with reduced intensity due to the early Atlantic profile bottom interactions (10–15 dB less). These principles were seen in many cases, but the types of propagation patterns they produced depended strongly on source depth via the relative amounts of sound in different modes. In some cases, primarily with shallower sources, the propagation patterns depended almost entirely on the sound-speed profile at the source. In other cases, usually with deeper sources, the propagation patterns were more determined by the destination water type.

This work confirms and extends the conclusion of Jensen *et al.* (1991) that, in the Iceland–Faeroes Gap region, the topographic configuration very strongly affects the acoustic propagation pattern. Use of contour plots of low-frequency sound magnitudes, and a more accurate sediment model, permits the interpretation that oceanographic variations produce significant but lesser modifications to local sound magnitudes by altering the amount of sediment interactions. We must note that these calculations were performed using a two-dimensional version of the acoustic model; due to the strong azimuthal dependence of both topography and oceanography, we can expect significant out-of-plane effects to occur in this region.

ACKNOWLEDGMENTS

The authors are greatly indebted to Professor William Siegmann of Rensselaer Polytechnic Institute and Professor George Frisk of Woods Hole Oceanographic Institute, whose many helpful discussions greatly assisted the inter-

pretations of this work. Dr. Ding Lee and Mr. George Botseas kindly provided the IFD model. This research was conducted under a Secretary of the Navy Graduate Fellowship in Oceanography (JCC) and supported by the Office of Naval Research under Grant N00014-90-J-1593 to Harvard University.

Akima, H. (**1970**). "A New Method of Interpolation and Smooth Curve Fitting Based on Local Procedures," J. Assoc. Comp. Mach. **17**, 589–602.

Botseas, G., Lee, D., and Gilbert, K. E. (**1983**). "IFD: Wide Angle Capability," NUSC Technical Report 6905.

Botseas, G., Lee, D. and Siegmann, W. L. (**1989**). "IFD: Interfaced with Harvard Open Ocean Model Forecasts," NUSC Technical Report 8367.

Carman, J. C. (**1991**). "Oceanographic and Topographic Interactions in Underwater Acoustic Propagation, with Regional Applications," Ph.D. thesis, Harvard University.

Carman, J. C. (**1994**). "Oceanographic, Topographic, and Sediment Interactions in Deep Water Acoustic Propagation: Part I—Sediment Effects on Water Column Propagation Patterns," J. Acoust. Soc. Am. **95**, 1344–1362.

Collins, M. D., Ali, H. B., Authement, M. J., Nagl, A., Überall, H., Miller, J. F., and Arvelo, J. I. (**1988**). "Low-Frequency Sound Interaction with a Sloping, Refracting Ocean Bottom," IEEE J. Oceanic Eng. **13**, 235–244.

Denbo, D. W., Robinson, A. R., Glenn, S. M., Walstad, L. J., and Mooney, C. (**1988**). "Harvard Gapcasts: Dynamical Nowcasts and Forecasts of the East Iceland-Faeroe Front July 1987," Harvard Open Ocean Model Reports 25, Rep. Meteor. Oceanogr., Harvard University.

Denbo, D. W., and Robinson, A. R. (**1988**). "Harvard Gapcasts; A Progress Report: Regional Forecasting, Processes and Methodology in the Iceland-Faeroe Island Gap. Part I: Data Forecast and Hindcast Experiments," Harvard Open Ocean Model Reports 32, Rep. Meteor. Oceanogr., Harvard University.

Denbo, D. W., and Robinson, A. R. (**1988**). "Harvard Gapcasts; A Progress Report: Regional Forecasting, Processes and Methodology in the Iceland-Faeroe Island Gap. Part II: GFD and Process Experiments," Harvard Open Ocean Model Reports 33, Rep. Meteor. Oceanogr., Harvard University.

Fofonoff, N. P., and Millard, Jr., R. C. (**1983**). "Algorithms for Computation of Fundamental Properties of Seawater," UNESCO Tech. Papers Marine Sci. **44**.

Frisk, G. V., Doutt, J. A., and Hays, E. E. (**1986**). "Geoacoustic Models for the Icelandic Basin," J. Acoust. Soc. Am. **80**, 591–600.

Hamilton, E. L. (**1980**). "Geoacoustic Modeling of the Sea Floor," J. Acoust. Soc. Am. **68**, 1313–1340.

Jensen, F. B., Dreini, G., and Prior, M. (**1991**). "Acoustic Effects of the Iceland–Faeroe Front," in *Ocean Variability and Acoustic Propagation* edited by J. R. Potter and A. Warn-Varnas (Kluwer Academic, Dordrecht, The Netherlands).

Jensen, F. B., and Kuperman, W. A. (**1980a**). "Range-Dependent Bottom-Limited Propagation Modeling with the Parabolic Equation" in *Bottom-Interacting Ocean Acoustics*, edited by W. A. Kuperman and F. B. Jensen (Plenum, New York).

Jensen, F. B., and Kuperman, W. A. (**1980b**). "Sound Propagation in a Wedge-Shaped Ocean with a Penetrable Bottom," J. Acoust. Soc. Am. **67**, 1564–1566.

Knobles, D. P., and Vidmar, P. J. (**1986**). "Simulation of Bottom Interacting Waveforms," J. Acoust. Soc. Am. **79**, 1760–1766.

Kuperman, W. A., and Jensen, F. B. (**1980**). *Bottom-Interacting Ocean Acoustics*, NATO Conference on Bottom-Interacting Ocean Acoustics, La Spezia, 1980 (Plenum, New York).

Lawrence, M. W. (**1983**). "Modeling of Acoustic Propagation across Warm-core Eddies," J. Acoust. Soc. Am. **73**, 474–485.

Lee, D., and Botseas, G. (**1982**). "IFD: An Implicit Finite-Difference Computer Model for Solving the Parabolic Equation," NUSC Tech. Rep. 6659.

Lee, D., Botseas, G., Siegmann, W. L., and Robinson, A. R. (**1989**). "Numerical Computations of Acoustic Propagation through Three-Dimensional Ocean Eddies," in *Numerical and Applied Mathematics*, edited by W. F. Ames (J. C. Baltzer AG, Scientific).

Levitus, S. (**1982**). *Climatological Atlas of the World Ocean*, NOAA Professional Paper No. 13, Rockville, MD.

Mellberg, L. E., Robinson, A. R., and Botseas, G. (**1990**). "Modeled Time Variability of Acoustic Propagation through A Gulf Stream Meander and Eddies," J. Acoust. Soc. Am. **87**, 1044–1054.

Miller, R. N., Robinson, A. R., and Haidvogel, D. B. (**1983**). "A Baroclinic Quasigeostrophic Open Ocean Model," J. Comp. Phys. **50**, 38–70.

Porter, M., Piacsek, S., Henderson, L., and Jensen, F. (**1990**). "Acoustic Impact of Upper Ocean Models," in *Proc. Second IMACS Symposium on Computational Acoustics*, edited by D. Lee, A. Cakmak, and R. Vichnevetsky (North-Holland, New York).

Potter, J. R., and Warn-Varnas, A. (Editors) (**1991**). *Ocean Variability and Acoustic Propagation* (Kluwer Academic, Dordrecht, The Netherlands).

Robinson, A. R. (**1983**). "Overview and Summary of Eddy Science," in *Eddies in Marine Science*, edited by A. R. Robinson (Springer-Verlag, Berlin).

Robinson, A. R., and Walstad, L. J. (**1987**). "The Harvard Open Ocean Model: Calibration and Application to Dynamical Process, Forecasting, and Data Assimilation Studies," Appl. Num. Math. **3**, 89–131.

Robinson, A. R., Walstad, L. J., Calman, J., Dobson, E. B., Denbo, D. W., Glenn, S. M., Porter, D. L., and Goldhirsh, J. (**1989**). "Frontal Signals East of Iceland from the GEOSAT Altimeter," Geophys. Res. Lett. **16**, 77–80.

Robinson, A. R. (**1992**). "Shipboard Prediction with a Regional Forecast Model," The Oceanography Soc. Mag. **5** (1), 42–48.

Robinson, A. R., Carman, J. C., and Glenn, S. M. (**1994**). "A Dynamical System for Acoustic Applications," in *Oceanography and Acoustics: Prediction and Propagation Models*, edited and with an introduction by A. R. Robinson and D. Lee (American Institute of Physics, New York).

Robinson, A. R., and Dobson, E. (**1989**). "Synoptic Variability of Frontal Meandering and Eddies from GEOSAT Altimetric Data East of Iceland," JHU/APL Report, SIR89U-035.

Siegmann, W. L., Jacobson, M. J., Lee, D., Botseas, G., Robinson, A. R., and Glenn, S. M. (**1990**). "Interfacing Mesoscale Ocean Prediction and Parabolic Acoustic Propagation Models Including Bottom Topography," in *Proc. Second IMACS Symposium on Computational Acoustics*, edited by D. Lee, A. Cakmak, and R. Vichnevetsky (North-Holland, New York).

Urick, R. J. (**1983**). *Principles of Underwater Sound* (McGraw-Hill, New York).

Vidmar, P. J. (**1980**). "The Effect of Sediment rigidity on Bottom Reflection Loss in a Typical Deep Sea Sediment," J. Acoust. Soc. Am. **68**, 634–638.